

Electric Field Effects on Short Fibrils of A β Amyloid Peptides

Francesca Lugli,^{*,†} Francesca Toschi,[†] Fabio Biscarini,[‡] and Francesco Zerbetto[†]

*Dipartimento di Chimica “G. Ciamician”, Università di Bologna, via F. Selmi 2,
40126 Bologna, Italy and ISMN CNR, V. Gobetti, Bologna, Italy*

Received December 2, 2009

Abstract: Amyloid fibrils are highly ordered protein aggregates, which are associated with many neurodegenerative diseases. The assembling dynamics of monomeric beta-amyloid peptides, A β , into small aggregates (and then into long fibrils) is still debated and has become a hot topic. In this study, we conducted molecular dynamics simulations in explicit water of small A β protofibrils (from monomer to pentamer) under the perturbation of an externally applied electric field with the aim of investigating the fundamental molecular interactions involved in the aggregation mechanism. Dynamics of small adducts of A β (16–42) in the presence of an electric field, which was shown before to accelerate the conformational change of a single molecule, indicate that the structural resilience increases with the number of molecules in the aggregate. In particular, for 50 ns, the pentamer shows an enhanced stability in secondary structure, number of hydrogen bonds, and number of salt bridges, even in the presence of the field perturbation. The resilience to the field perturbation is linked to the variation of the induced dipole moment of the aggregates that tends to level off very rapidly with the growing number of molecules, thereby reducing the energy available per molecule to produce structural changes. The results also show that in the presence of the field the stability of the hydrophobic second β -sheet (β 2, residues 31–42) is higher than that of the first one (β 1, residues 18–26). In particular, we identify Gly33, Gly37, and Met35 as the most important residues that stabilize the intermolecular packing and may act as nucleation sites for fibrillization. Furthermore, dynamics of the full-length A β (1–42) pentameric aggregate, which include the highly charged random coil residues 1–15, confirmed the key role of the second hydrophobic core in the protofibril structure.

1. Introduction

The interest in amyloid fibrils arises because of their association with neurodegenerative diseases, including Alzheimer’s disease (AD), type 2 diabetes, prion diseases, Parkinson’s disease, senile systemic amyloidosis, and Huntington’s disease.^{1–3} Amyloid diseases are characterized by extracellular deposition of insoluble plaques of misfolded polypeptides aggregated into ordered fibril structures. X-ray diffraction from amyloid fibrils shows that, despite differ-

ences in the amino acid sequence, they share a common cross- β structural motif, where β -strands run perpendicular to the long axis of the fibrils while the hydrogen bonds between β -strands are parallel to the axis.⁴

The major component of the amyloid plaques of AD is the 39–42-residue-long amyloid- β (A β) peptide, which is generated from the amyloid precursor protein by the proteolytic activities of β - and γ -secretase.⁵ It has been shown that before fibril formation, natively unstructured monomeric A β peptide undergoes large conformational changes from a high α -helix content peptide into a spherical amyloid intermediate, which contains predominantly β -sheet structures.⁶ Small A β oligomers show higher toxicity than the fibril, indicating that the β -sheet formation may trigger

* To whom correspondence should be addressed. Tel.: +39 051 2099915. Fax: +39 051 2099456. E-mail: francesca.lugli@unibo.it.

[†] Università di Bologna.

[‡] ISMN CNR.

neurotoxicity.^{7–10} It is also known that A β 42 is more prone to aggregation than the shorter A β 40.^{11–13}

Understanding the molecular mechanisms of A β amyloid fibril formation and its early detection is important in the elucidation of the role of endogenous factors that may inhibit amyloidogenesis in the normal brain and/or promote it in the AD brain and could also play a role in the design and development of new types of ultrastrong materials because of the high mechanical toughness of the fibrils.¹⁴ Prerequisite to the elucidation of the pathway of aggregation is the understanding of the thermodynamics of the aggregation process and in particular of the conformational rearrangements that carry the starting proteins to the product A β amyloid fibril. Perturbations of the thermodynamics properties of a protein in its soluble or its fibrillar state are usually measured by solid-state NMR spectroscopy, Fourier-transform IR, circular dichroism, gel filtration, electron microscopy, etc., but do not necessarily correlate with the aggregation pathway.¹⁵ Structural information about the fibrils comes primarily from electron microscopy images, X-ray diffraction, solid-state NMR, and biochemical studies.^{16–18} On the basis of such experimental observations, several atomic models for amyloid fibril structure have been proposed.^{19–22} They show that the N-terminal segment, where polar residues are located, exhibits a disordered structure, whereas the C-terminal segment is more ordered and characterized by two hydrophobic β -strands connected by a turn. These two β -sheets are constructed by residues 18–26 (β 1) and residues 31–42 (β 2), while the loop comprises residues 27–30 (see Figure 1).

Experimental studies, supported by computer simulations, have shown that also fragments of A β can form fibrils. In particular, simulations performed on β -strand segments such as A β _{10–35}, A β _{16–35}, and A β _{29–42} peptides^{23,24} form in register parallel β -sheets, while A β _{34–42} and A β _{16–22} prefer an antiparallel organization.^{18,25,26} In the model proposed by Ma and Nussinov²³ the key structural feature of the salt bridge between Asp23–Lys28 is illustrated, along with the intramolecular hydrophobic cluster between Leu17/Phe19 and Ile32/Leu34.

Nussinov and co-workers performed several MD simulations investigating the protofibril structure and stability of A β _{17–42} in linear-like²⁷ and annular-like structures.²⁸ It has also been shown that while fibrillar A β amyloids are always organized in a parallel β -sheet conformation, small oligomeric A β display an antiparallel β -sheet structure.²⁹ Here, we investigate only a fibrillar-like arrangement.

Molecular dynamics simulations of long protofilaments, not considered here, confirmed the role of strong hydrophobic interactions between the β -strands for the stability of the fibril structure.³⁰ Recently, the aggregation behavior of small protofibrillar aggregates (from dimer to pentamer) of A β _{17–42} was studied by MD simulations, suggesting that the second hydrophobic β -strand may act as the nucleation site for aggregation.³¹ The role of the β 2 portion in stabilizing small aggregates and possibly inducing the growth of fibrils was also confirmed by MD simulations performed on the full-length A β (1–42).³²

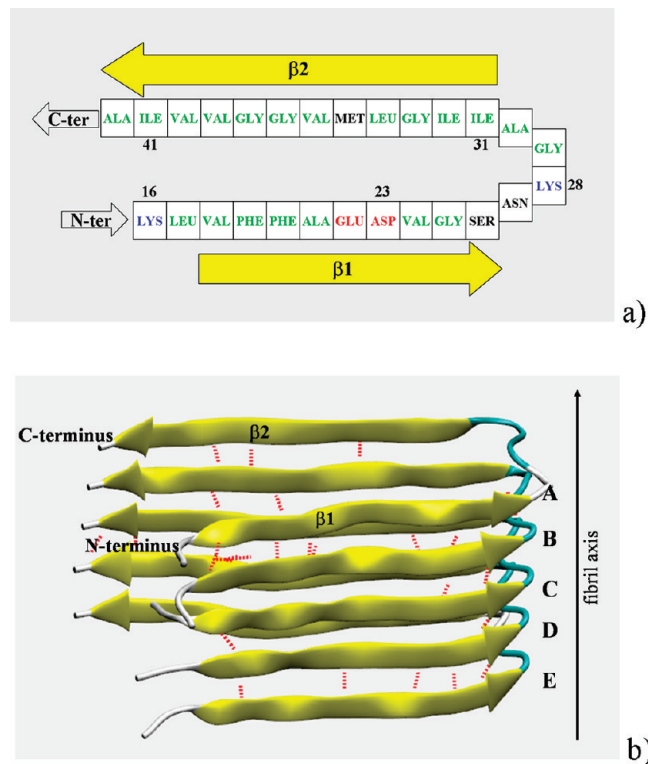


Figure 1. (a) Amino acid sequence of A β (16–42). The hydrophobic residues are in green, positively and negatively charged residues are in blue and red, respectively, while polar residues are in black. β -Sheets, β 1 and β 2, are also indicated. (b) The 3D structure of A β pentamer. Ribbon diagram of the core structure of residues 16–42 showing the intermolecular nature of the inter- β -strands interactions. Red dotted lines indicate the intermolecular H bonds. Individual molecules are labeled as A, B, C, D, and E.

The early detection of the amyloid aggregates could also be important for an early diagnosis of the disease and could be obtained by transistor-based sensors.^{33–35} Structural and functional modifications of biosystems by electromagnetic field exposure are also a growing concern for society. For instance, a recent study showed evidence of nonthermal microwave damage of brain tissue in exposed rats.³⁶ Microwave radiation was shown to induce changes in protein conformations and to promote formation of amyloid fibrils in vitro under nonphysiological conditions.³⁷ Electric fields and electric potentials also have therapeutical effects in deep brain stimulation techniques, where the application of relatively small voltages (~1–3 V) by an electrode implanted in the brain is used to treat Parkinson's disease symptoms.³⁸ Changes in electrical fields associated with membranes can play a role in diseases such as Alzheimer's.^{39,40}

To the best of our knowledge, the possible use of an electric field to influence or modify the strong interactions that exist in amyloid fibrils has not yet been considered. It therefore appears important to investigate the behavior of biosystems under an external electric field (EF). In particular, analysis of the modifications of the structure of individual proteins, their aggregates, and the aggregation mechanism are of practical interest. Computational approaches are rapidly becoming inexpensive and accurate tools to perform such investigation. We recently studied the effect of an

electric field on the coil-to- β sheet conversion of the amyloid peptide,⁴¹ with an approach similar to that of Budi et al.^{42–44} We also investigated the effect of an electric field on a nanosize water drop deposited on a surface⁴⁵ and the effect of water on the response of an organic field effect transistor.⁴⁶ In this work, we examine the early response of small amyloid protofibrils to an externally applied electric field. The external electric field is set to 0.5 V/nm (and in one case to 0.25 V/nm) since this magnitude was shown to be close to the limit of instability of water and strongly modified the conformation of a single amyloid peptide in water.^{41,47}

2. Methods

2.1. Structural Model. The starting structures were extracted from the model, deposited in the Protein Data Bank, whose PDB code is 2BEG.²⁰ The 3D structure of the Alzheimer's A β (1–42) protofilament was obtained using hydrogen-bonding constraints from quenched hydrogen/deuterium-exchange NMR, side-chain packing constraints from pairwise mutagenesis studies, and parallel, in-register β -sheet arrangement from previous solid-state NMR studies. The model contains 10 structures of a pentamer of the β -amyloid (17–42) peptides. The first 16 residues are disordered, and the 3D structure contains coordinates of the core structure of residues 17–42.

For the calculations, the first structure of the pentamer was extracted. At each molecule the residue Lys16 was added in order to neutralize the system. In this way, each molecule contains two negatively charged residues (Glu22 and Asp23) and two positively charged residues (Lys16 and Lys28).

The peptides A β (16–42) were terminated by an acetyl group at the N-terminus and by N-methyl group at the C-terminus. Figure 1 shows the amino acid sequence and the starting structure of the β -amyloid protofilament.

The core of the amyloid fibril is composed of two β -sheets (β 1 and β 2) whose strands are perpendicular to the fibril axis and hydrogen bonds between peptides that run roughly parallel to the axis. The first, β 1, comprises residues Val18–Ser26, residues Gly27–Ala30 form a turn, residues Ile31–Ala42 form the second strand, β 2. Asp23 and Lys28 form a salt bridge, which has been shown in previous computational studies²³ to be fundamental for the fibril structure and in the stabilization the U-shape of the peptide.

The systems simulated were the monomer (molecule A), the dimer adduct (molecules A and B), the trimer adduct (molecules A, B, and C), the tetramer adduct (molecules A, B, C, and D), and pentamer adduct (molecules A, B, C, D, and E) in water boxes of 64 Å side lengths containing about 8000 water molecules.

2.2. Molecular Dynamics. The calculations were performed with the NAMD 2.6 Molecular Dynamics program⁴⁸ using periodic boundary conditions and cubic simulation cells. Electrostatic interactions were calculated with the particle mesh Ewald (PME) method^{49–51} with a grid spacing of 1.2 Å and a spline interpolation of order 4. We used a cutoff of 12 Å for the real-space direct sum part of the Ewald sum and for the van der Waals interactions. The time integration step was set to 2 fs. Simulations at 300 K were

carried out for all systems. Rigid bonds involving hydrogen atoms were constrained using the SHAKE algorithm.⁵² The force field adopted is CHARMM27⁵³ for the peptide, whereas water is modeled by the TIP3P force field.⁵⁴ The calculations were carried out in steps: (a) minimization of the lateral chains, with the backbone frozen; (b) minimization of the water molecules, with the whole protein frozen; (c) minimization of the entire system, with the backbone frozen; (d) MD equilibration in the NVT ensemble for 250 ps with the backbone frozen; (e) MD equilibration in the NPT for 250 ps with the backbone frozen, pressure set to 1 atm, and by using the Langevin dynamics,⁵⁵ (f) MD simulation in the NPT ensemble, where systems were coupled to a barostat with a constant pressure set to 1 atm and a relaxation time of 0.1 ps and to a Berendsen thermostat with temperature set to 300 K.⁵⁶ The validity of this procedure has been confirmed in previous studies.^{41,43} For each of the smallest adducts (dimer, trimer, and tetramer), two 10 ns long molecular dynamics, MD, simulations were performed in the absence and in the presence of a constant external electric field (EF) of 0.5 V/nm, while for the pentamer adduct simulations up to 50 ns were carried out. In all systems, the electric field was applied along the direction of the fibril axis. In order to verify whether the direction of the EF influences the energy and stability of the structures, an additional MD run was performed on the pentamer adduct with the EF perpendicular to the fibril axis. As a reference, two 5 ns long MD simulations (with and without EF) were run for the monomer.

In order to check whether the highly charged and polar N-terminal random coil segment (1–15) influences the structural stability of the core β -sheet domain, three 50 ns MD simulations of the full-length A β (1–42) pentamer were carried out: with electric fields of 0.25 and 0.5 V/nm and without electric field. This system was built adding the random coil segment (1–15) to the five peptides of the equilibrated A β (16–42) pentamer structure.

2.3. Analysis Tools. The structural stability of the systems under the influence of an external applied field was investigated by determining, as a function of time, the root-mean-square deviations (rmsd) from the structure at the start of the data collection. Also, the radius of gyration (R_g) was examined. The rmsd was calculated only for the C_α atoms, after their least-squared superposition with the initial positions. We also analyzed the time evolution of secondary, tertiary, and quaternary structures. The site-specific propensity for secondary structure formation is determined by the STRIDE program⁵⁷ in the VMD software package.⁵⁸ STRIDE contains a knowledge-based algorithm that uses hydrogen-bond energy and statistically derived backbone torsional angle information to return the secondary structure assignments in maximal agreement with crystallographic designations. Information about tertiary and quaternary structures were obtained by analyzing the intramolecular and intermolecular contact maps. Contacts between pairs of amino acids can be visualized by using contact maps, 2D representations of all amino acid pairs in contact and where contact frequencies are represented by different colors. The intramolecular contact map only takes into account the contacts between pairs of amino acids in the same peptide and

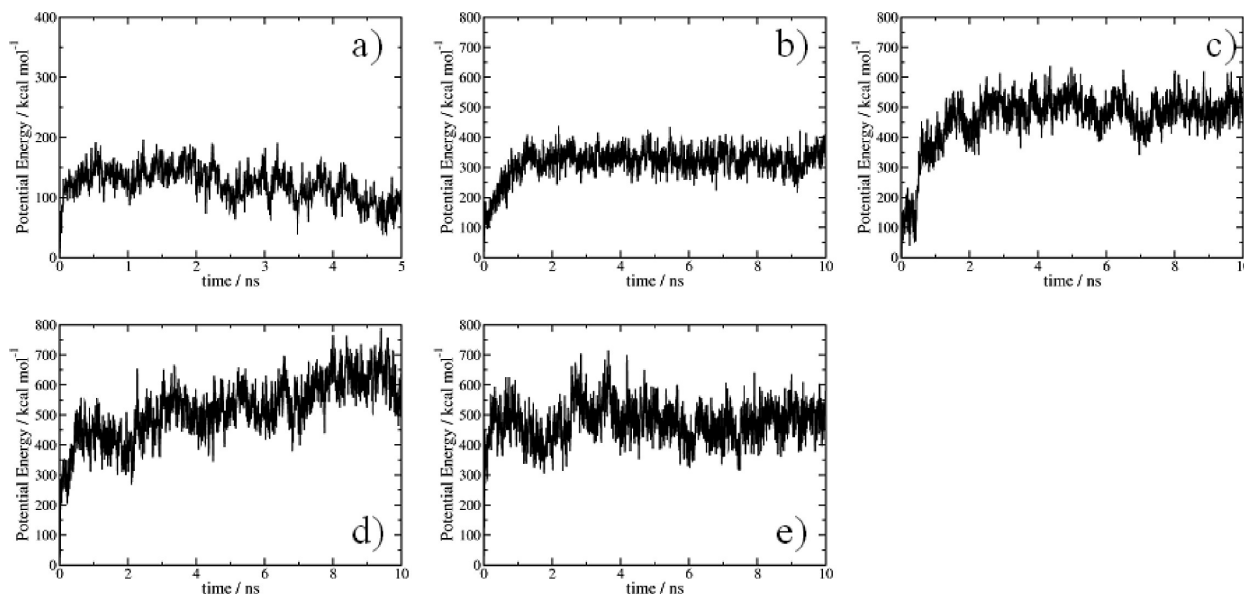


Figure 2. Evolution in time of the energy: (a) monomer, (b) dimer, (c) trimer, (d) tetramer, and (e) pentamer aggregates after an external EF of 0.5 V/nm is switched on. For simplicity, the initial energy is taken as a reference and set to zero.

contains information about the tertiary structure of peptides within the aggregates. The intermolecular contact map only takes into account the contacts between pairs of amino acids that belong to different peptides and yields information on the way different peptides assemble into the aggregate (the quaternary structure). The salt bridges distances were monitored in time by using the VMD Salt Bridges plugin. A salt bridge is considered formed if the distance between the oxygen atom of an acidic residue and the nitrogen atom of a basic residue is within the cutoff distance (default 3.2 Å). Hydrogen bonds are quantified by counting acceptor atom–donor atom pairs that are no further than 3.0 Å and within a cutoff angle of 20°. Total dipole moments of the aggregates were also calculated in time.

3. Results and Discussion

3.1. Electric Field Effect on A β (16–42) Protomibrils.

The early response of small A β (16–42) protomibrils to a strong electric field (EF = 0.5 V/nm) was first analyzed in terms of potential energy profiles in a time range of 10 ns, see Figure 2. The change of potential energy of the A β (16–42) adducts is related to the structural destabilization of the systems due to the field perturbation. The initial energy, at the time when the field is switched on, is taken as a reference and set to zero. The field changes the potential energy of systems and quickly destabilizes them by \sim 142 kcal mol⁻¹ for the monomer, \sim 326 kcal mol⁻¹ for the dimer, \sim 489 kcal mol⁻¹ for the trimer, \sim 581 kcal mol⁻¹ for the tetramer, and \sim 470 kcal mol⁻¹ for the pentamer. It is instructive to notice that the increase of potential energy destabilization is linear with the number of peptides in the adducts up to the tetramer while the destabilization of the pentamer is less than that calculated for the tetramer. In the absence of the field, the average value of the potential energy is $0.5k_BT$ per degree of freedom. The activation of the field introduces forces that act on the charges and the dipoles present in the simulation box. It is reasonable to expect that

at equilibrium, the effect of the forces is to distort the molecules and increase the total potential energy, proportionally to the number of atoms. The pentamer “stabilization” in the presence of the EF with respect to the other aggregates means that its structural conformation is less affected by the external perturbation.

The root-mean-square deviations (rmsds) of positions of the C_α atoms relative to the initial structure of each molecule labeled as A, B, C, D, and E (see Figure 1b) in the dimeric, trimeric, tetrameric, and pentameric aggregates are shown in Figure 3. For each molecule, comparison of the behavior in the presence and in the absence of an electric field, EF, of 0.5 V/nm is possible. The size of the electric field was selected on the basis of previous molecular dynamics simulations performed on the monomer, where 0.5 V/nm showed an acceleration of the denaturation of the peptide in water in 10 ns.⁴¹

In general, application of the electric field affects the smaller aggregates. The effect of the electric field is quite small in the pentamer. The average rmsd values for each of the adducts averaged after equilibration are shown in Table 1 and concur with the more detailed profiles shown in Figure 3. Furthermore, one can notice that the dimer is not stable even without perturbation, and the main effect of the application of the external field is to accelerate the conformational destabilization.

The average radius of gyration (R_g) of each system is also given in Table 1. Only the dimeric and trimeric adducts modify their shape in the presence of the field while tetramer and pentamer tend to retain it.

Figure 4 compares the maps of the evolution of the secondary structure as a function of time both in the absence and in the presence of the field. Noticeable differences appear for the smaller systems when the field is present. In general, also for the larger aggregates, the EF increases the number of residues with a turn conformation. In the pentamer, only the top molecule A (see Figure 1b) is affected, an effect due

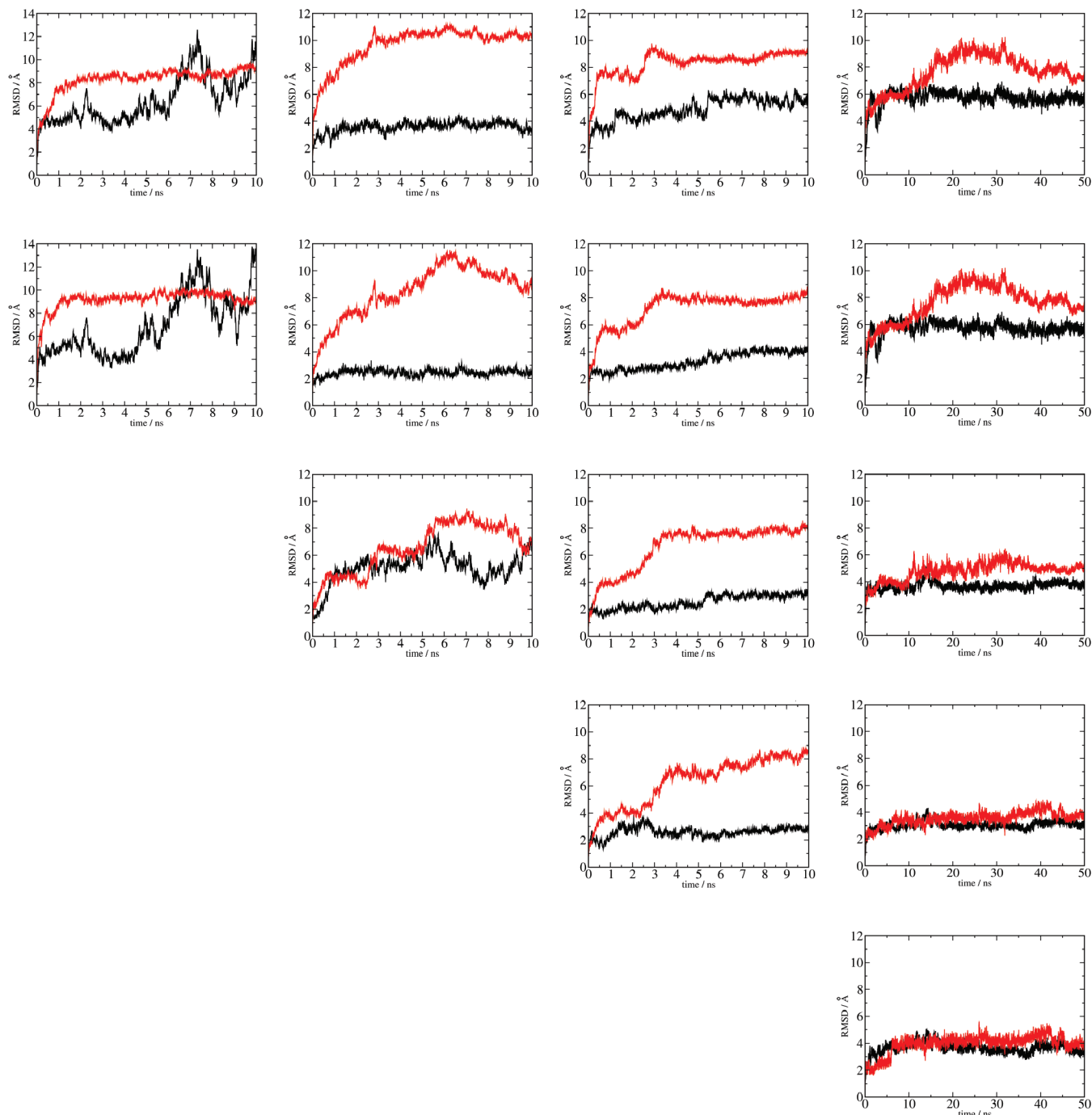


Figure 3. Evolution of the rmsd of C_α atoms. From top to bottom, A, B, C, D, and E molecules in the aggregates. From left to right, dimeric, trimeric, tetrameric, and pentamer aggregates. The molecules in each aggregate are labeled from A to E (see Figure 1): (black line) simulation in the absence of the EF, (red line) simulation in the presence of the EF of 0.5 V/nm.

Table 1. RMSDs (\AA) and Radius of Gyration (\AA) Averaged after Equilibration

system	rmsd (\AA), no EF	rmsd (\AA), EF = 0.5 V/nm	R_g (\AA), no EF	R_g (\AA), EF = 0.5 V/nm
monomer	8.5 ± 0.7	10.6 ± 0.4	11.6 ± 0.5	11.7 ± 0.6
dimer aggregate	8.9 ± 1.6	9.1 ± 0.2	16.1 ± 1.3	11.3 ± 0.1
trimer aggregate	4.1 ± 0.4	10.4 ± 0.9	14.4 ± 0.1	13.2 ± 0.4
tetramer aggregate	3.9 ± 0.2	8.1 ± 0.3	14.3 ± 0.1	14.1 ± 0.2
pentamer aggregate	6.0 ± 0.2	6.9 ± 0.3	14.9 ± 0.1	15.1 ± 0.3

to the lack of stabilizing interactions (such as intermolecular salt bridges) with monomers above it.

A good hydrophobic side-chain packing pattern is essential for maintaining the stable β -sheet conformation. Contact

maps can help to rationalize this aspect. Stable and strong hydrophobic lateral chain contacts contribute to stabilize the β -sheet secondary structure, maintaining the hydrogen-bond network between different molecules in the adducts.

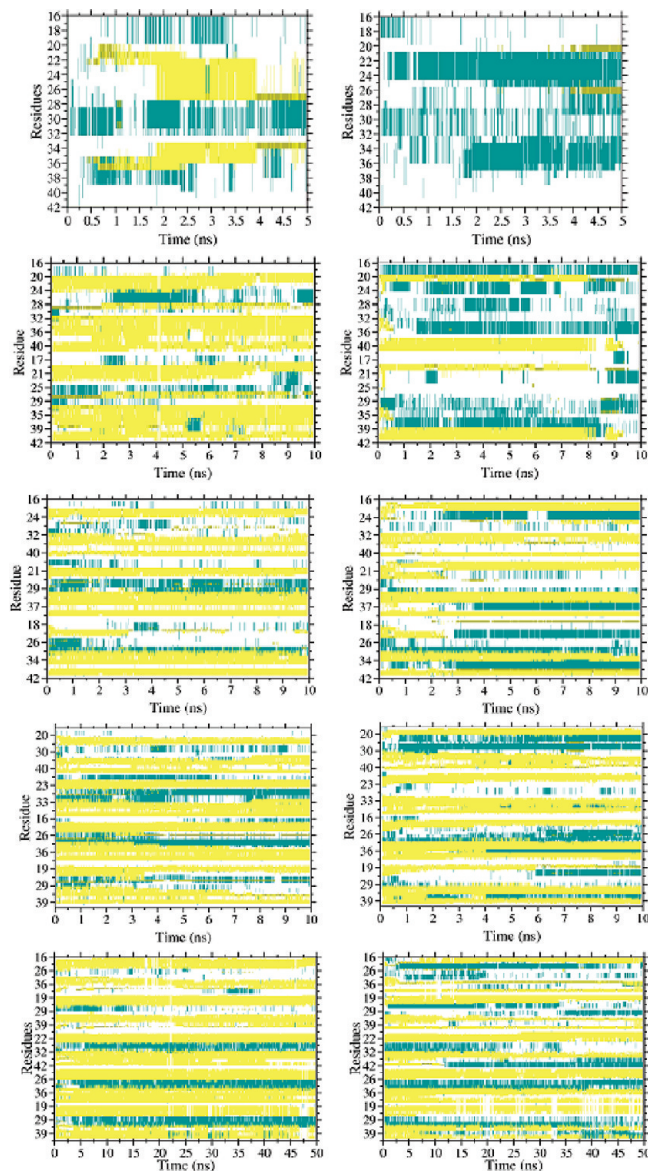


Figure 4. Maps of the evolution of the secondary structure as a function of time. Top to bottom: monomer, dimer, trimer, tetramer, and pentamer. (Left) No electric field; (right) EF = 0.5 V/nm. The vertical axis contains the residue number of the 16–42 A β sequence. Yellow for β -sheet, ochre and green for turn, and white for coil.

Figure 5 displays the average intramolecular (tertiary structure) and intermolecular (quaternary structure) contact maps for each system. Each pixel in the maps represents the contact strength between two residues. In the intramolecular maps (first and second vertical entries, labeled “Intramolecular”), vertical and horizontal axes represent residues of the same molecule (the dark diagonals are the contact of each residue with itself). The maps are symmetric with respect to the diagonal. The extradiagonal dark pixels represent the intersheet contacts between β 1 and β 2 of the same molecule, which are slightly influenced by the field. In particular, the tertiary structure is stabilized by intersheet side-chain interactions between residues Phe19/Gly38 and Ala21/Val36 and by intramolecular salt bridges between residues Asp23 and Lys28. The intermolecular maps (third and fourth vertical entries, labeled “Intermolecular”) repre-

sent contacts between residues of the n th molecule (vertical axis) and the $(n-1)$ th one (horizontal axis). The diagonals represent the distance between the same residues of vicinal molecules, and the maps are not necessarily symmetric. The pentameric protofilament is stabilized by intermolecular side-chain interactions between the odd-numbered residues of sheet $\beta 1$ of the n th molecule and the even-numbered residues of the sheet $\beta 2$ of the $(n-1)$ th molecule (see the dark pixels in the bottom-right region of the contact map) and, more importantly, by salt bridges between residues Asp23 and Lys28. These results are in agreement with the experimental model proposed by Lührs et al.²⁰ The electric field effect will necessarily be smaller in the case of hydrophobic contacts.

The intermolecular salt bridges have a preferential orientation. They form between Asp23 of the n th molecule and Lys28 of the $(n - 1)$ th one. The direction of the EF coincides with the fibril axis and should stabilize the intermolecular salt bridges.

The intramolecular salt bridges are affected by the field and tend to be disrupted by the field (see Table 1 in the Supporting Information). The noticeable exception is the pentameric adduct, where, in 50 ns, the bridges of the inner molecules remain stable in the presence of the field. These resilient bridges hold the shape of the molecule in place so that the gyration radius (and the rmsd) of Table 1 and Figure 3 do not vary in the presence of the field.

The intermolecular salt bridges are disrupted by the field in the dimeric and trimeric aggregates. However, they are quite stable in the two higher adducts. Peculiarly, a salt bridge that opposes the field is formed in the tetramer. The simplest explanation for its presence is that the local electrostatic effect wins over the nonlocal perturbation of the field, which orients the adduct along its direction in less than 100 ps, see Table 2, and tends to increase the overall dipole moment. Table 2 shows that the dipole moment of the adducts, in the presence of the field, reaches a limiting value already for the trimer and that alignment with the field is very rapid.

The higher resilience of the intermolecular salt bridges, with respect to the intramolecular ones, can be explained by considering the orientation of the dipole moment, which is aligned along the direction of the intermolecular salt bridges and creates a stabilizing interaction when the field is switched on.

Applying the field along the perpendicular direction of the fibril axis effects only the time, τ , required to align the dipole moment of the system to the field but effects neither the potential energy nor the structural features of the aggregates.

The convergence of the dipole moment properties offers a simple explanation for the stability of the aggregates. The interaction energy between the dipole moment and the electric field, $\mu \cdot E$, reaches a plateau already for the trimer adduct. This is the energy available to modify the shape of the adduct, either at the molecular level or its overall shape. Increasing the size of the adduct, the energy available from the field becomes negligible once smeared out over the individual molecules.

The rigidity of the systems is evident if one considers the number of hydrogen bonds present during the dynam-

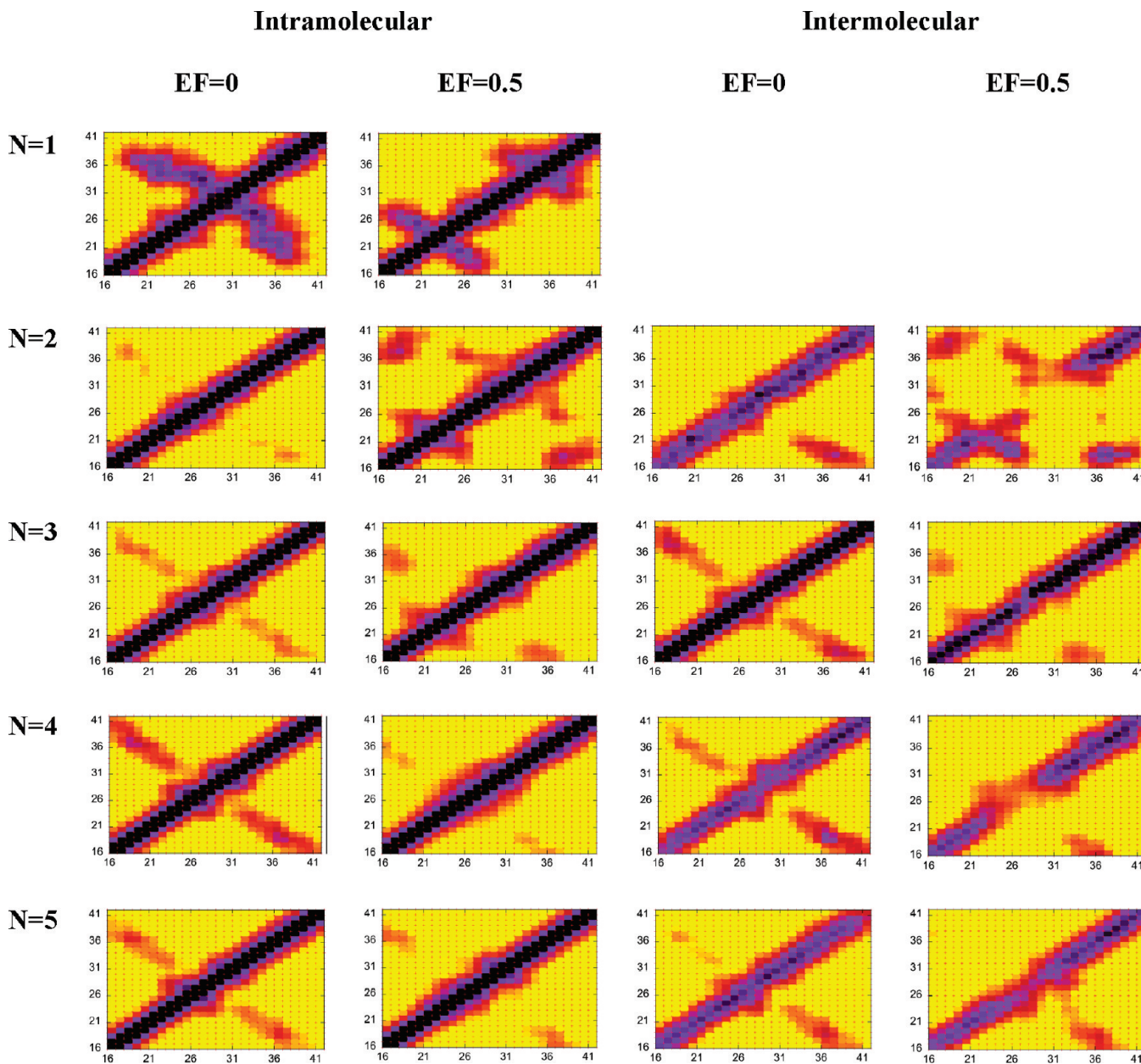


Figure 5. Intramolecular and intermolecular contact maps. Both the x and y axes have the residues number in the peptide $\text{A}\beta_{16-42}$ sequence. Top to bottom: monomer ($N = 1$), dimer adduct ($N = 2$), trimer adduct ($N = 3$), tetramer adduct ($N = 4$), pentamer adduct ($N = 5$). Left to right, first entry intramolecular contact maps with no electric field, second entry intramolecular contact maps with $\text{EF} = 0.5 \text{ V/nm}$, third entry intermolecular contact maps with no electric field, and fourth entry intermolecular contact maps with $\text{EF} = 0.5 \text{ V/nm}$. Each pixel in the maps represents the average contact strength between two residues and is color coded: yellow, no contact; orange, red, magenta, to violet, strong contacts; black, very strong contact.

Table 2. Summary of the Dipole Moments, in Debyes, Averaged after Equilibration, and Time, τ in ps, Required To Align the Adduct with the Field

system	μ , no EF	μ , EF = 0.5 V/nm	μ_z , no EF off	μ_z , EF = 0.5 V/nm	τ
monomer	100 ± 30	296 ± 7	18 ± 23	250 ± 6	30
dimer adduct	138 ± 36	539 ± 9	-105 ± 57	536 ± 10	50
trimer adduct	149 ± 28	780 ± 12	-22 ± 75	778 ± 12	50
tetramer adduct	288 ± 19	850 ± 20	230 ± 43	821 ± 17	90
pentamer adduct	470 ± 31	924 ± 19	-343 ± 96	915 ± 19	70

ics, see Table 3. The electric field halves their number in the dimeric aggregate but barely affects it in the higher adducts.

The stability of intermolecular hydrogen bonds in larger adducts is also responsible for the stability of secondary

structure. Previous DFT calculations showed that intermolecular hydrogen bonds formed between the β -sheets of stacked amyloid peptides in the fibril are strongly cooperative and probably may contribute to the nucleation growth kinetics observed experimentally.⁵⁹

Table 3. Number of Hydrogen Bonds Averaged after Equilibration

system	no EF			EF = 0.5 V/nm		
	total	intra	inter	total	intra	inter
monomer	1.3 ± 0.9			0.7 ± 0.7		
dimer adduct	7.4 ± 2.3	0.3 ± 0.5	7.1 ± 2.3	4.1 ± 2.2	0.3 ± 0.6	3.8 ± 2.2
trimer adduct	12.1 ± 2.9	0.2 ± 0.4	11.9 ± 2.8	10.9 ± 2.6	1.1 ± 0.9	9.8 ± 2.5
tetramer adduct	21.0 ± 3.4	2.3 ± 1.0	18.7 ± 3.4	18.1 ± 3.6	1.2 ± 0.8	16.9 ± 3.6
pentamer adduct	30.9 ± 6.1	3.0 ± 1.3	27.9 ± 6.1	28.1 ± 4.9	3.4 ± 1.4	24.7 ± 5.9

The β -sheet content per residue, calculated along the 10 ns MD runs and averaged over all the molecules, is shown in Figure 6. In the absence of the field the β -sheet content increases with the number of monomers. The extension of $\beta 1$ increases upon going from trimer to tetramer to pentamer, while $\beta 2$ is almost stable for all the adducts, and the β -strand segment, 39–41, is slightly lower for the pentamer. The effect of the EF is to decrease the extension of $\beta 1$, while $\beta 2$ exhibits higher secondary structural stability; residues Val40 and Ile41 increase their β -sheet content.

The results are consistent with a recent study, where the stability of $A\beta(17-42)$ aggregates was investigated by MD simulations at high temperature,³¹ and also with experimental and theoretical studies which indicated the importance of Ile41 for paranucleus formation in $A\beta 42$.^{60,61}

The segment $\beta 2$ has a higher hydrophobic content than $\beta 1$. Hydrophobic residues such as Ile, Leu, and Met are known to exhibit a positive contribution to protein stability. A good side-chain packing is fundamental for maintaining a stable secondary β -sheet structure because it protects the hydrogen-bonding network from water solvation.⁶² By analyzing inter- and intramolecular contact maps, one can notice that the strongest contacts are between the hydrophobic residues, which are perturbed the least by EF.

These findings imply that hydrophobic interactions play an important role in maintaining the secondary structural stability of the $A\beta$ fibrils, also in presence of external perturbation. The stable β -sheet structure also explains the stabilization of the number of intermolecular hydrogen bonds.

3.2. Simulations of the Full-Length $A\beta(1-42)$ Pentamer. The application of an external perturbation confirms that the strong hydrophobic interactions between the β -strands

are the critical element in maintaining the amyloid fibril stability. This holds also when a full-length $A\beta(1-42)$ protofibril, which contains the highly charged N-terminal residues, is affected by the electric field perturbation.

The effect of an externally applied electric field of 0.5 V/nm on the pentameric $A\beta(1-42)$ was analyzed in terms of root-mean-square displacements of different peptide regions, namely, the random coil, RC (residues 1–17), the first β -sheet, $\beta 1$ (residues 18–26), the turn (residues 27–30), and the second β -sheet, $\beta 2$ (residues 31–42). The results, averaged over the five molecules of the protofibril, are displayed in Figure 7. The field mainly affects the highly charged random coil portion, causing the consequent structural deformation also of the $\beta 1$ region, which is increasingly disrupted. On the contrary, the hydrophobic $\beta 2$ region remains stable during the simulation.

Figure 8 shows the comparison of the time evolution of the secondary structure between $A\beta(16-42)$ and $A\beta(1-42)$. The main effect of the EF is to decrease the β -sheet content in the $\beta 1$ segment of the full-length $A\beta(1-42)$. After ~20 ns, such β -sheet content goes nearly to zero while the $\beta 2$ segment shows resistance to the field. In particular, residues Leu34-Met35 and Val40-Ile41 are the most resilient in both pentamers.

The intermolecular contact map averaged over the last 20 ns of simulation (Figure 9) confirms that the most resilient hydrophobic contacts are located in the $\beta 2$ segment. In particular, contact pairs Gly33-Gly33, Gly37-Gly37, and Met35-Met35 remain relatively stable. These results agree with previous studies³¹ that suggested that these contacts trigger the β -sheet packing during the early stages of aggregation.

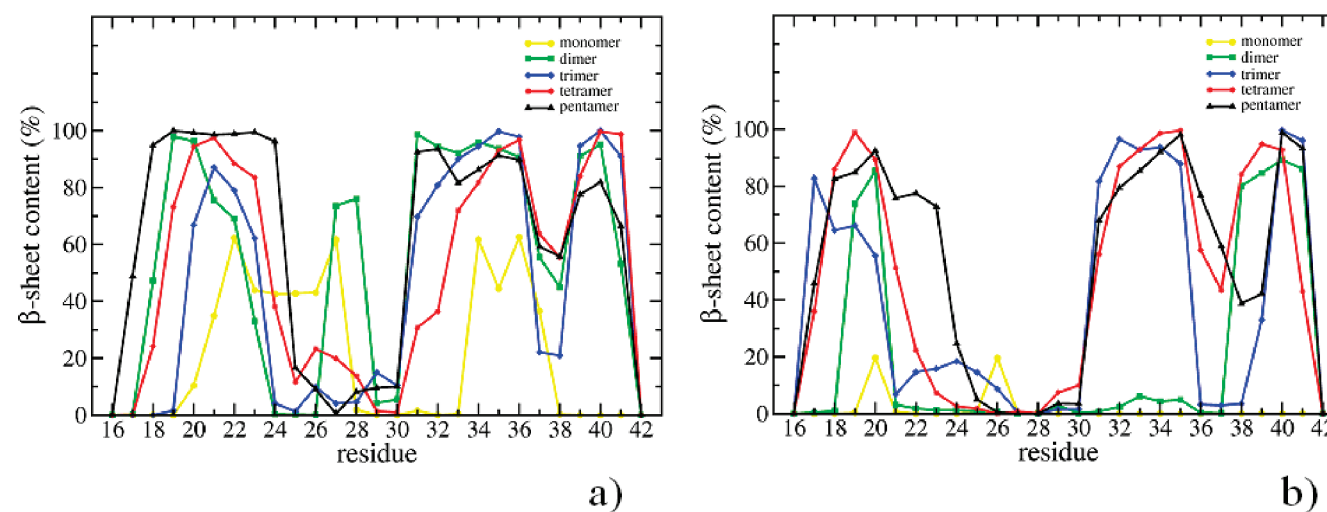


Figure 6. β -Sheet content per residue (a) without electric field and (b) with an applied electric field of 0.5 V/nm.

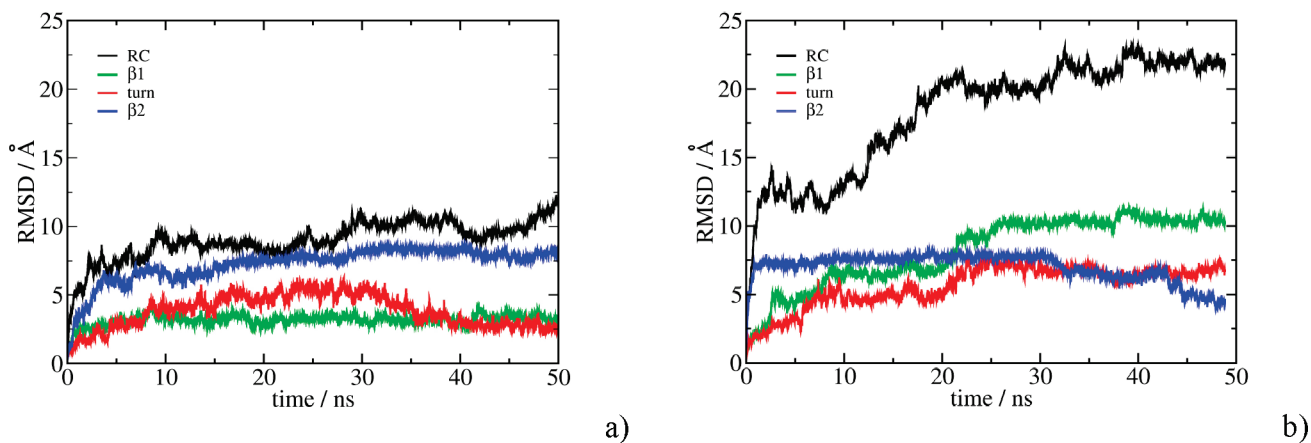


Figure 7. rmsd as a function of time, calculated for the $\text{A}\beta(1\text{--}42)$ pentamer (a) without EF and (b) with $\text{EF} = 0.5 \text{ V/nm}$.

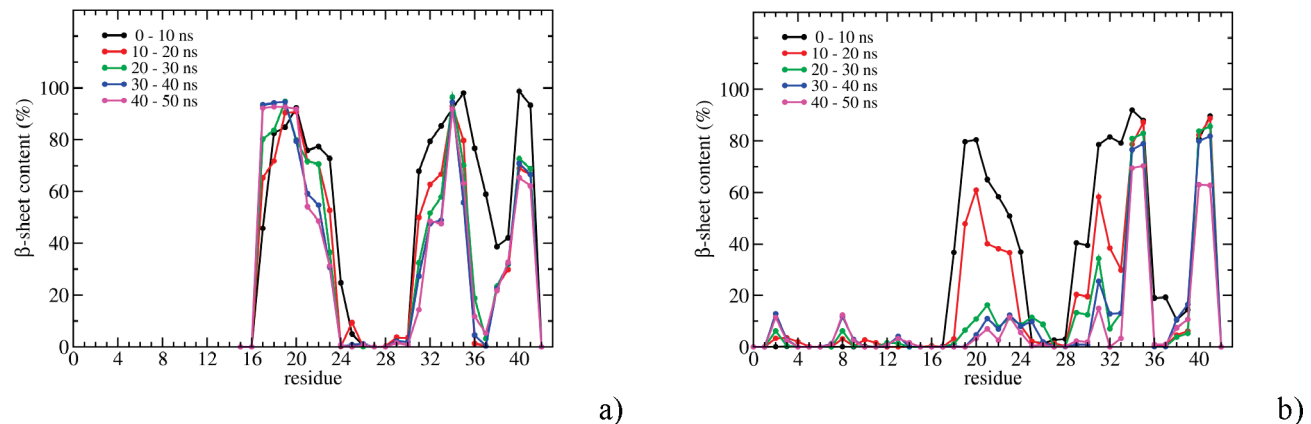


Figure 8. Time evolution of the β -sheet content for all residues (a) in the pentameric adduct of $\text{A}\beta(16\text{--}42)$ and (b) in the pentameric adduct $\text{A}\beta(1\text{--}42)$, both under $\text{EF} = 0.5 \text{ V/nm}$.

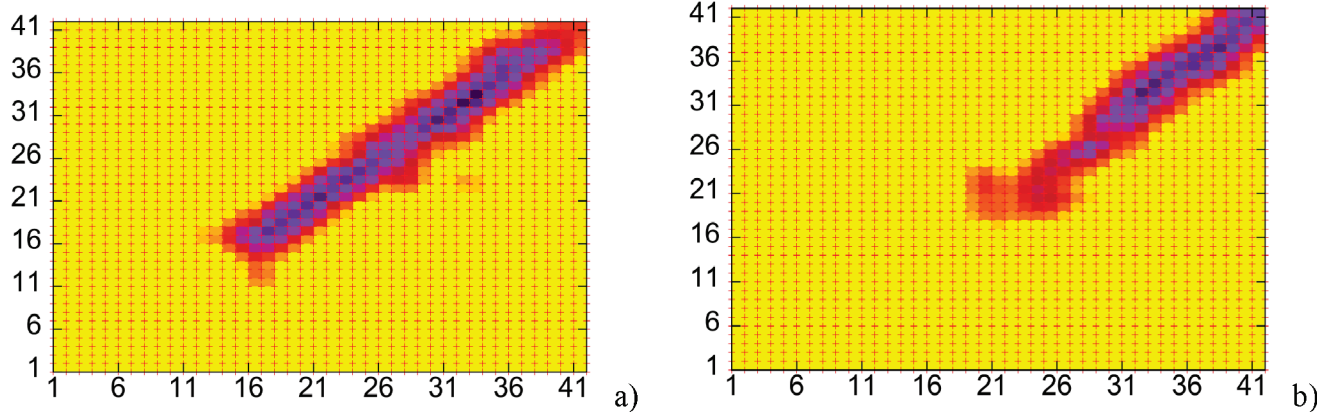


Figure 9. Intermolecular contact maps of the pentameric $\text{A}\beta(1\text{--}42)$ averaged over the five molecules and the last 20 ns of simulation (a) in the absence and (b) in the presence of EF. The x and y axes contain the residue number in the peptide $\text{A}\beta_{1\text{--}42}$ sequence. Each pixel in the map represents the contact strength between two residues and is color coded: yellow, no contact; orange, red, magenta, to violet, strong contacts; black, very strong contact.

The electric field mainly acts on the charged residues. Since the charged residues are located in the region of random coil and $\beta 1$, the effect is to “stretch” the molecules. Only two internal salt bridges are stable for the 50 ns of the simulation, namely, those between molecules B and C and between molecules C and D. The intermolecular hydrogen-bond network of $\beta 1$ is slowly reduced, while the H bonds of the $\beta 2$ region are preserved. Representative pictures of

the pentameric $\text{A}\beta(16\text{--}42)$ and $\text{A}\beta(1\text{--}42)$ during the simulations are provided in the Supporting Information.

The effect of a different field strength on the full-length $\text{A}\beta(1\text{--}42)$ pentameric aggregate was also investigated. Since electric fields larger than 0.5 V/nm encounter water instability,^{41,42} which is manifested as an explosion of the water box, we performed a further 50 ns long MD simulation of the pentameric adduct $\text{A}\beta 42$ under a field of 0.25 V/nm.

Also, in this case, the most internal monomers (molecules B and C) are the most stable. The major difference with the previous simulation, see plots similar to Figures 8 in the Supporting Information, is a partial resilience of the β_1 segment, where residues 18–26 conserve their β -sheet conformation for a longer time.

4. Conclusion

Amyloid proteins may undergo a structural transition from the native soluble monomeric conformation to fibrillar assemblies that have predominantly β -sheet structure.

The study of the principal driving forces that maintain the aggregate state of $A\beta$ peptides is a key issue not only for the understanding of pathological mechanisms involved in many neurodegenerative diseases but also for the development of new nanomaterials that can resist external mechanical perturbation.

The use of modified physiological conditions, such as temperature, pressure, pH, or solvents, has been shown to be a useful tool to study protein aggregation stability. The application of external fields can also be used to rationalize the most important interactions in the formation of amyloid aggregates.

In this study, we conducted numerical simulations of the smallest aggregates of $A\beta(16–42)$ peptides under the perturbation of an electric field. We show that the stability of the aggregates increases with the number of monomers and that larger protofibrils tend to resist to electric field perturbations for at least 50 ns. The number of H bonds and salt bridges is not affected by a field large enough to accelerate the coil-to- β -sheet conformational conversion of the monomer.⁴¹ The overall shape and position of the individual atoms of the adducts are also weakly affected by the electric field. Only some turns are introduced.

In the case of the full-length $A\beta(1–42)$ pentameric adduct, which carries a net negative charge, the main effect of the electric field is to decrease the amount of the β -sheet content in the β_1 segment, leading to a destabilization of intermolecular contact pairs in the N-terminal region (residues 1–21). The hydrophobic β_2 segment is less affected by the strong field, and residues 33–35 and 40–42 tend to maintain their native intermolecular contact pairs.

The present results concur with the hypothesis that the hydrophobic β_2 segment may act as a nucleation site during early stages of $A\beta$ aggregation.

Acknowledgment. We are grateful to Pablo Stolar, Dago de Leeuw, and Arian Shehu for stimulating discussions. This work was supported by the project EU-STRP 0032652 BIODOT.

Supporting Information Available: Dynamics observed in the simulations for the salt bridges, both intramolecular and intermolecular; results of the 50 ns long MD simulations performed on the pentameric $A\beta(1–42)$ adduct with an electric field of 0.25 V/nm; representative pictures of $A\beta(16–42)$ and $A\beta(1–42)$ pentamers during the simulations. This material is available free of charge via the Internet at <http://pubs.acs.org>.

References

- (1) Rochet, J.-C.; Lansbury, P. T. *Curr. Opin. Struct. Biol.* **2000**, *10*, 60–68.
- (2) Selkoe, D. J. *Nature* **1999**, *399*, A23–A31.
- (3) Selkoe, D. J. *Neuron* **1991**, *6*, 487–498.
- (4) Sunde, M.; Blake, C. *Adv. Protein Chem.* **1997**, *50*, 123–159.
- (5) Yankner, B. A. *Neuron* **1996**, *16*, 921–932.
- (6) Chimon, S.; Shaibat, M. A.; Jones, C. R.; Calero, D. C.; Aizezi, B.; Ishii, Y. *Nat. Struct. Mol. Biol.* **2007**, *14*, 1157–1164.
- (7) Bucciantini, M.; Giannoni, E.; Chiti, F.; Baroni, F.; Formigli, L.; Zurdo, J.; Taddei, N.; Ramponi, G.; Dobson, C. M.; Stefani, M. *Nature* **2002**, *416*, 507–511.
- (8) Bucciantini, M.; Calloni, G.; Chiti, F.; Formigli, L.; Nosi, D.; Dobson, C. M.; Stefani, M. *J. Biol. Chem.* **2004**, *279*, 31374–31382.
- (9) Hardy, J.; Selkoe, D. J. *Science* **2002**, *297*, 353–356.
- (10) Walsh, D. M.; Klyubin, I.; Fadeeva, J. V.; Cullen, W. K.; Anwyl, R.; Wolfe, M. S.; Rowan, M. J.; Selkoe, D. J. *Nature* **2002**, *416*, 535–539.
- (11) Jarrett, J. T.; Berger, E. P.; Lansbury, P. T. *Biochemistry* **1993**, *32*, 4693–4697.
- (12) Bitan, G.; Kirkpatrick, M. D.; Lomakin, A.; Vollmers, S. S.; Benedek, G. B.; Teplow, D. B. *Proc. Natl. Acad. Sci. U.S.A.* **2003**, *100*, 330–335.
- (13) Harper, J. D.; Wong, S. S.; Lieber, C. M.; Lansbury, P. T. *Chem. Biol.* **1997**, *4*, 119–125.
- (14) Cherny, I.; Gazit, E. *Angew. Chem., Int. Ed.* **2008**, *47*, 4062–4069.
- (15) Kim, Y. S.; Liu, L.; Axelsen, P. H.; Hochstrasser, R. M. *Proc. Natl. Acad. Sci. U.S.A.* **2008**, *105*, 7720–7725.
- (16) Balbach, J. J.; Petkova, A. T.; Oyler, N. A.; Antzutkin, O. N.; Gordon, D. J.; Meredith, S. C.; Tycko, R. *Biophys. J.* **2002**, *83*, 1205–1216.
- (17) Sachse, C.; Fändrich, M.; Grigorieff, N. *Proc. Natl. Acad. Sci. U.S.A.* **2008**, *105*, 7462–7466.
- (18) Balbach, J. J.; Ishii, Y.; Antzutkin, O. N.; Leapman, R. D.; Rizzo, N. W.; Dyda, F.; Reed, J.; Tycko, R. *Biochemistry* **2000**, *39*, 13748–13759.
- (19) Petkova, A. T.; Ishii, Y.; Balbach, J. J.; Antzutkin, O. N.; Leapman, R. D.; Delaglio, F.; Tycko, R. *Proc. Natl. Acad. Sci. U.S.A.* **2002**, *99*, 16742–16747.
- (20) Lührs, T.; Ritter, C.; Adrian, M.; Riek-Lohr, D.; Bohrmann, B.; Döbeli, H.; Schubert, D.; Riek, R. *Proc. Natl. Acad. Sci. U.S.A.* **2005**, *102*, 17342–17347.
- (21) Nelson, R.; Eisenberg, D. *Curr. Opin. Struct. Biol.* **2006**, *16*, 260–265.
- (22) Tycko, R. *Curr. Opin. Struct. Biol.* **2004**, *14*, 96–103.
- (23) Ma, B.; Nussinov, R. *Proc. Natl. Acad. Sci. U.S.A.* **2002**, *99*, 14126–14131.
- (24) Itoh, S. G.; Okamoto, Y. *J. Phys. Chem. B* **2008**, *112*, 2767–2770.
- (25) Klimov, D. K.; Thirumalai, D. *Structure* **2003**, *11*, 295–307.
- (26) Favrin, G.; Irbäck, A.; Mohanty, S. *Biophys. J.* **2004**, *87*, 3657–3664.

- (27) Zheng, J.; Jang, H.; Ma, B.; Tsai, C.-J.; Nussinov, R. *Biophys. J.* **2007**, *93*, 3046–3057.
- (28) Zheng, J.; Jang, H.; Ma, B.; Nussinov, R. *J. Phys. Chem. B* **2008**, *112*, 6856–6865.
- (29) Cerf, E.; Sarroukh, R.; Tamamizu-Kato, S.; Breydo, L.; Derclaye, S.; Dufrêne, Y. F.; Narayanaswam, V.; Goormaghtigh, E.; Ruysschaert, J.-M.; Raussens, V. *Biochem. J.* **2009**, *421*, 415–423.
- (30) Buchete, N.-V.; Tycko, R.; Hummer, G. *J. Mol. Biol.* **2005**, *353*, 804–821.
- (31) Zhao, J.-H.; Liu, H.-L.; Liu, Y.-F.; Lin, H.-Y.; Fang, H.-W.; Ho, Y.; Tsai, W.-B. *J. Biomol. Struct. Dyn.* **2009**, *26*, 481–490.
- (32) Masman, M. F.; Eisel, U. L. M.; Csizmadia, I. G.; Penke, B.; Enriz, R. D.; Marrink, S. J.; Luiten, P. G. M. *J. Phys. Chem. B* **2009**, *113*, 11710–11719.
- (33) Katz, E.; Willner, I. *Electroanalysis* **2003**, *15*, 913–947.
- (34) Heller, I.; Janssens, A. M.; Mannik, J.; Minot, E. D.; Lemay, S. G.; Dekker, C. *Nano Lett.* **2007**, *8*, 591–595.
- (35) Zhou, X.; Moran-Mirabal, J. M.; Craighead, H. G.; McEuen, P. L. *Nat. Nanotechnol.* **2007**, *2*, 185–190.
- (36) Salford, L. G. B. A. E.; Eberhardt, J. L.; Malmgren, L.; Persson, B. R. R. *Environ. Health Perspect.* **2003**, *111*, 881.
- (37) de Pomerai, D. I.; Smith, B.; Dawe, A.; North, K.; Smith, T.; Archer, D. B.; Duce, I. R.; Jones, D.; Candido, E. P. M. *FEBS Lett.* **2003**, *543*, 93–97.
- (38) Benabid, A. L. *Curr. Opin. Neurobiol.* **2003**, *13*, 696–706.
- (39) Blanchard, B. J.; Thomas, V. L.; Ingram, V. M. *Biochem. Biophys. Res. Commun.* **2002**, *293*, 1197–1203.
- (40) Tyner, K. M.; Kopelman, R.; Philbert, M. A. *Biophys. J.* **2007**, *93*, 1163–1174.
- (41) Toschi, F.; Lugli, F.; Biscarini, F.; Zerbetto, F. *J. Phys. Chem. B* **2009**, *113*, 369–376.
- (42) Budi, A.; Legge, F. S.; Treutlein, H.; Yarovsky, I. *J. Phys. Chem. B* **2005**, *109*, 22641–22648.
- (43) Budi, A.; Legge, F. S.; Treutlein, H.; Yarovsky, I. *J. Phys. Chem. B* **2007**, *111*, 5748–5756.
- (44) Budi, A.; Legge, F. S.; Treutlein, H.; Yarovsky, I. *J. Phys. Chem. B* **2008**, *112*, 7916–7924.
- (45) Cramer, T.; Zerbetto, F.; García, R. *Langmuir* **2008**, *24*, 6116–6120.
- (46) Cramer, T.; Steinbrecher, T.; Koslowski, T.; Case, D. A.; Biscarini, F.; Zerbetto, F. *Phys. Rev. B* **2009**, *79*, 155316.
- (47) Xu, D.; Phillips, J. C.; Schulten, K. *J. Phys. Chem.* **1996**, *100*, 12108–12121.
- (48) Phillips, J. C.; Braun, R.; Wang, W.; Gumbart, J.; Tajkhorshid, E.; Villa, E.; Chipot, C.; Skeel, R. D.; Kale, L.; Schulten, K. *J. Comput. Chem.* **2005**, *26*, 1781–1802.
- (49) Darden, T.; York, D.; Pedersen, L. *J. Chem. Phys.* **1993**, *98*, 10089–10092.
- (50) Essmann, U.; Perera, L.; Berkowitz, M. L.; Darden, T.; Lee, H.; Pedersen, L. G. *J. Chem. Phys.* **1995**, *103*, 8577–8593.
- (51) Petersen, H. G. *J. Chem. Phys.* **1995**, *103*, 3668–3679.
- (52) Ryckaert, J.-P.; Ciccotti, G.; Berendsen, H. J. C. *J. Comput. Chem.* **1977**, *23*, 327–341.
- (53) MacKerell, A. D.; Bashford, D.; Bellott, Dunbrack, R. L.; Evanseck, J. D.; Field, M. J.; Fischer, S.; Gao, J.; Guo, H.; Ha, S.; Joseph-McCarthy, D.; Kuchnir, L.; Kuczera, K.; Lau, F. T. K.; Mattos, C.; Michnick, S.; Ngo, T.; Nguyen, D. T.; Prodhom, B.; Reiher, W. E.; Roux, B.; Schlenkrich, M.; Smith, J. C.; Stote, R.; Straub, J.; Watanabe, M.; Wiorkiewicz-Kuczera, J.; Yin, D.; Karplus, M. *J. Phys. Chem. B* **1998**, *102*, 3586–3616.
- (54) Jorgensen, W. L.; Chandrasekhar, J. r; Madura, J. D.; Impey, R. W.; Klein, M. L. *J. Chem. Phys.* **1983**, *79*, 926–935.
- (55) Feller, S. E.; Zhang, Y.; Pastor, R. W.; Brooks, B. R. *J. Chem. Phys.* **1995**, *103*, 4613–4621.
- (56) Berendsen, H. J. C.; Postma, J. P. M.; van Gunsteren, W. F.; DiNola, A.; Haak, J. R. *J. Chem. Phys.* **1984**, *81*, 3684–3690.
- (57) Frishman, D. A. P. *Proteins: Struct. Funct. Genet.* **1995**, *23*, 566–579.
- (58) Humphrey, W.; Dalke, A.; Schulten, K. *J. Mol. Graphics* **1996**, *14*, 33–38.
- (59) Tsemekhman, K.; Goldschmidt, L.; Eisenberg, D.; Baker, D. *Protein Sci.* **2007**, *16*, 761–764.
- (60) Bitan, G.; Vollers, S. S.; Teplow, D. B. *J. Biol. Chem.* **2003**, *278*, 34882–34889.
- (61) Urbanc, B.; Cruz, L.; Yun, S.; Buldyrev, S. V.; Bitan, G.; Teplow, D. B.; Stanley, H. E. *Proc. Natl. Acad. Sci. U.S.A.* **2004**, *101*, 17345–17350.
- (62) Röhrig, U. F.; Laio, A.; Tantalo, N.; Parrinello, M.; Petronzio, R. *Biophys. J.* **2006**, *91*, 3217–3229.

CT1001335